

A Novel Garment Transfer Method Supervised by Distilled Knowledge of Virtual Try-on Model

Naiyu Fang^a, Lemiao Qiu^{a,*}, Shuyou Zhang^a, Zili Wang^a, Kerui Hu^a,
Jianrong Tan^a

^a*State Key Laboratory of Fluid Power & Mechatronic Systems, Zhejiang University, Hangzhou, 310027, China*

Abstract

When a shopper chooses garments online, garment transfer technology wears the garment from the model image onto the shopper’s image, allowing the shopper to decide whether the garment is suitable for them. As garment transfer leverages wild and cheap person image as garment condition, it has attracted tremendous community attention and holds vast commercial potential. However, since the ground truth of garment transfer is almost unavailable in reality, previous studies have treated garment transfer as either pose transfer or garment-pose disentanglement, and trained garment transfer in self-supervised learning, yet do not cover garment transfer intentions completely. Therefore, the training supervising the garment transfer is a rock-hard issue. Notably, virtual try-on technology has exhibited superior performance using self-supervised learning. We supervise the garment transfer training via knowledge distillation from virtual try-on. Specifically, we first train the transfer parsing reasoning model at multi-phases to provide shape guidance for downstream tasks. The transfer parsing reasoning model learns the response and feature knowledge from the try-on parsing reasoning model and absorbs the hard knowledge from the ground truth. By leveraging the warping knowledge from virtual try-on, we estimate a progressive flow to precisely warp the garment by learning the shape and content correspondence. To enhance transfer realism, we propose a well-designed arm regrowth task to infer exposed skin pixel content. Experiments demonstrate that our method has state-of-the-art performance in transferring garments between

*Corresponding author

Email address: qiulm@zju.edu.cn (Lemiao Qiu)

person compared with other virtual try-on and garment transfer methods.

Keywords:

Garment Transfer, Knowledge Distillation, Virtual Try-on, Parsing Reasoning, Garment Warping

1. Introduction

Virtual try-on wears the garment-in-shop into a person, while garment transfer wears the garment from one person to another. As Fig. 1 shows, the garment-in-shop of virtual try-on is captured in a controlled environment using professional techniques, while the person image of garment transfer is wilder and cheaper. In a word, garment transfer also allows shoppers to perceive the garment-wearing effect but does not require specific and expensive garment conditions. However, the pair of garment-in-shop and the try-on result is easy to collect, and the pair of the person image and the transfer result is almost unavailable. Thus, garment transfer is a user-friendly but training-hard topic. As virtual try-on is implemented by self-supervised learning and both technologies share the same purpose, we propose to supervise the training of garment transfer by distilling knowledge from virtual try-on. To the best of our knowledge, this is the first time to implement garment transfer via knowledge distillation. In this paper, we present a novel garment transfer pipeline and knowledge distillation process by exploiting previous virtual try-on studies.

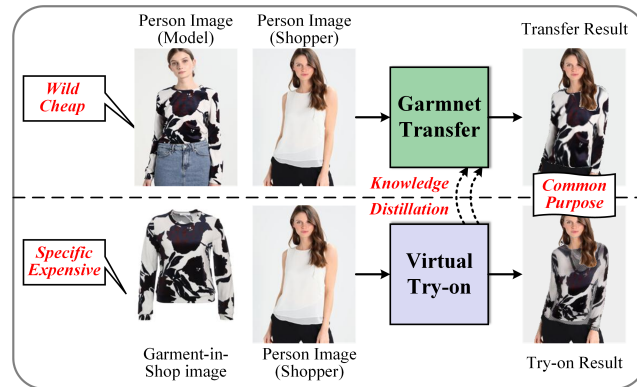


Figure 1: Garment transfer vs virtual try-on.

To wear a garment-in-shop, the virtual try-on method warps the garment-in-shop towards the person’s pose and preserves the other person’s features. It involves many topics, such as image warping, image synthesis, and image fusion. VITON [1] proposed the concept of image-based virtual try-on for the first time and provided an inspiring pipeline to implement it. It synthesizes a coarse try-on result, warps the garment-in-shop toward this result, and combines the synthesized and warped results to refine the garment texture. Alternatively, CP-VTON [2] offers a different pipeline where the warping and synthesis sequences are reversed. Since the paired garment-in-shop and the try-on result are available, they were both trained in a self-supervised manner by wearing a garment-in-shop onto a person dressed in the same garment. This self-supervision learning enables models to develop warping and rendering capacities that can handle new garment-wearing cases during the testing phase.

Intuitively, the garment input of virtual try-on is nearly aligned and has a high pixel ratio since it is captured at a hanging status in the shop. Conversely, the garment in the person image is entangled with the pose feature of the person, presenting challenges for the garment transfer model. When two persons wear different garments in various poses, the ideal ground truth for garment transfer is for one person to wear the other person’s garment and maintain its intrinsic pose. However, it is almost impossible to collect such ground truth data in reality. Therefore, the primary focus of garment transfer studies is on how to supervise its learning, and there are two dominant ways to achieve this. One approach [3] is to disentangle the garment in person image from pose and train the model in a self-supervised manner to reconstruct the person image conditioned on the spatial-agnostic garment and pose features. The other approach [4] is to directly alter the pose feature of the garment by warping. With a pair of person images where a person wears the same garment but has different poses, the model is trained to warp the garment from one pose to another.

Since pair fashion data is essential for the training of virtual try-on and garment transfer, several public datasets have been released for research purposes. The Zalando dataset [1] contains the paired garment-in-shop and try-on result images in a resolution of 256×256 . A similar virtual try-on dataset [5] is collected but in a higher resolution of 1024×768 . Deepfashion2 [6] provided paired person images with different poses in the in-shop clothes retrieval benchmark, which has been extensively employed for self-supervised learning of garment transfer and pose transfer issues.

With the easy-to-access dataset and easy-to-follow pipeline, virtual try-on studies are more flourishing than garment transfer studies. Existing garment transfer studies encounter several issues that hinder their ability to achieve transfer results comparable to virtual try-on studies. 1) The self-supervised learning does not completely conform to its intention. The disentanglement of garment and pose is not imperative to garment transfer and impose a burden on models in reconstructing high-frequency details when re-entangling the garment and pose. These studies typically train garment transfer as pose transfer within the same person, leading to shape and style preservation issues when transferring garments to other person; 2) The task execution sequence is unreasonable. As the traditional learning methods cannot supervise the training of transfer parsing reasoning conditioned on transferred garment and person image, transfer parsing reasoning only follows garment warping and guides final image synthesis. Without transfer parsing prior, garment transfer guided by target pose is inevitable to yield misalignment and artifacts. 3) A specialized preservation mechanism for person features is missing. Both direct propagation and content inference are required in transferring the person’s features, such as the face and skin texture, into the final result. However, they only consider the direct composition of the warped garment and person image without designing specialized mechanisms to handle the multi-tasks involved in person feature preservation.

To address these issues, we propose a novel garment transfer method where the training is supervised by virtual try-on via knowledge distillation. It just adopts the existing virtual try-on dataset and does not require paired person images. It is trained in a fully supervised manner so that the input conditions of the training and testing phase are identical. And knowledge distillation is employed during training transfer parsing reasoning and garment warping. We summarize the main contributions of our paper as follows:

(1) Teaching transfer parsing reasoning in multi-phase. The transfer parsing reasoning model learns the response and feature knowledge from the pre-trained try-on parsing reasoning model in garment transfer. We then transfer the garment back to its originator so that the transfer parsing reasoning model absorbs the hard knowledge from the ground truth to improve its robustness.

(2) Supervising garment warping with the shape and content information. We first map the garment to a similar position to the target shape. With the warping knowledge of garment-in-shop, a progressive flow is estimated to precisely warp the garment by learning the correspondence at both the

shape and content level.

(3) Experiments demonstrate that our method has state-of-the-art performance compared other the virtual try-on and garment transfer methods in garment transfer. Our method performs well in transfer parsing reasoning, garment warping, new skin inference, and final result synthesis whatever the dressing and pose of person images are.

2. Related Work

Virtual Try-on VITON [1] and CP-VTON [2] determined the fundamental strategy to implement virtual try-on, and the subsequent studies focused on optimizing garment warping and person reservation. Yang H et al. introduced second-order constraint into the TPS deformation in ACGPN [7]. Minar M R et al. proposed CP-VTON+ [8] extended on CP-VTON where the skin label is updated and the garment-in-shop mask is concatenated into the image synthesis. Neuberger A et al. [9] proposed an online optimization step to optimize fine details reservation. Ge C et al. introduced cycle consistency to implement self-supervision learning in DCTON [10]. However, the coarse-grained TPS deformation used by these methods inevitably results in misalignment between the garment and person, requiring warping and rendering to be combined, which can introduce artifacts into the final result. To address this issue, some studies have used optical flow with higher DOF for finer warping. Ge Y et al. proposed PF-AFN [11] to estimate appearance flow from coarse to fine. He S et al. [12] proposed Flow Style VTON (FSV) to estimate a global warping tendency via style modulation based on PF-AFN. Additionally, some studies have used knowledge distillation to make their models independent of parsing and pose. Issenhuth T et al. proposed WUTON [13] to transfer warping knowledge and disambiguate the human parser error influence. PF-AFN [11] and FSV [12] linked the teacher model output with the student model input to implement the parser-free virtual try-on.

Garment Transfer It is regarded as garment-pose disentanglement or pose transfer for self-supervised learning. For the former, as the originator of garment transfer, SwapNet [3] learned the categories embedding by ROI pooling to disentangle the garment with the pose. Xie Z et al. proposed PASTA-GAN [14] to cut the garment into multiple patches for the disentanglement and exploited two StyleGAN2 to re-entangle garment patches with pose while considering style and texture. For the latter, Yang F et al. pro-

posed two complementary warping in CT-Net [4] to implement garment pose changing. Liu T et al. proposed SPATT [15] to establish a spatial correspondence in UV space to facilitate garment warping and unobserved region inference.

Knowledge Distillation It was proposed by Hinton G et al. in [16], where the pre-trained teacher model supervises the student model learning by teaching various knowledge. This approach aims to compress the parameter quantity and training data, enabling the student model to be lightweight. The distilled knowledge can be categorized into three types: response knowledge, feature knowledge, and relation knowledge. Specifically, response knowledge [16] and feature knowledge [17] are extracted at the last and hint layer, containing prediction and processing information. And relation knowledge [18] describes the relationship between data or feature maps. The methods of knowledge distillation are categorized into offline distillation, online distillation, and self-distillation. Offline distillation employs a large model pre-trained on a large dataset as the teacher model and teaches a lightweight student model. In contrast, online distillation [19] synchronously trains the teacher and student models to achieve better knowledge transfer when the large model is unavailable for specific tasks. Because of its universality and flexibility, knowledge distillation has been applied in several domains, including multi-view learning [20] and speaker extraction [21].

3. Methodology

3.1. Outline

We describe that the garment is transferred from person A to person B . Assuming that the image of person A and B are \mathcal{I}_A and \mathcal{I}_B , the corresponding garment-in-shop A and B are \mathcal{I}_A^c and \mathcal{I}_B^c , virtual try-on intends to wear \mathcal{I}_B^c onto \mathcal{I}_A , while garment transfer intends to transfer garment \mathcal{I}_B^{hc} from \mathcal{I}_B to \mathcal{I}_A . Since it is easy to collect the paired data $(\mathcal{I}_A, \mathcal{I}_A^c)$, the virtual try-on model can be trained in a self-supervised manner. Conversely, the paired data $(\mathcal{I}_A, \mathcal{I}_B, \mathcal{I}_{AB})$ is almost unavailable in the real world, it is a rock-hard issue to supervise the training of garment transfer. As they share a common objective, we endeavor to conduct the training of garment transfer by distilling knowledge from virtual try-on.

As Fig. 2 shows, we exploit the same pipeline for virtual try-on and garment transfer: parsing reasoning, garment warping, arm regrowth, and remaining content propagation. Virtual try-on teaches garment transfer

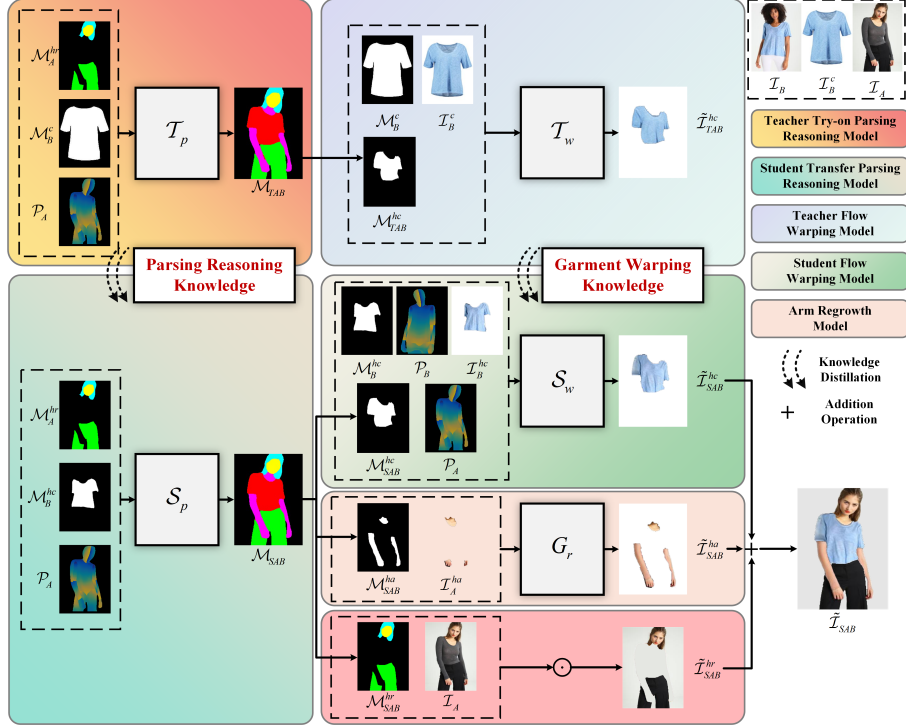


Figure 2: The outline of the proposed method. We distill the parsing reasoning and garment warping knowledge in parsing reasoning and garment warping. Following training, S_p is capable of reasoning \mathcal{M}_{SAB} to guide the downstream tasks, and S_w estimates a refined flow that warps \mathcal{I}_B^{hc} towards \mathcal{M}_{SAB}^{hc} . We concatenate $\tilde{\mathcal{I}}_{SAB}^{hc}$, $\tilde{\mathcal{I}}_{SAB}^{ha}$, and $\tilde{\mathcal{I}}_{SAB}^{hr}$ to yield final transfer result $\tilde{\mathcal{I}}_{SAB}$.

via knowledge distillation in the parsing reasoning and garment warping tasks. For virtual try-on, the teacher transfer parsing reasoning model T_p and teacher flow warping model T_w are trained in a self-supervised manner. In the testing phase, T_p reasons the try-on parsing \mathcal{M}_{TAB} where person A wears the garment-in-shop B . Guided by the garment mask \mathcal{M}_{TAB}^{hc} of \mathcal{M}_{TAB} , T_w warps \mathcal{I}_B^c towards \mathcal{M}_{TAB}^{hc} to yield $\tilde{\mathcal{I}}_{TAB}^{hc}$. For garment transfer, the student transfer parsing reasoning model S_p and the student flow warping model S_w are trained with supervision information distilled from T_p and T_w . S_p reasons the transfer parsing \mathcal{M}_{SAB} where person A wears the garment of person B (Sec. 3.2). With this target shape \mathcal{M}_{SAB}^{hc} , S_w warps garment \mathcal{I}_B^{hc} to yield $\tilde{\mathcal{I}}_{SAB}^{hc}$ (Sec. 3.3). For the transfer realism, the arm regrowth model G_r reasons more upper body skin $\tilde{\mathcal{I}}_{SAB}^{ha}$ when $\mathcal{M}_{SAB}^{ha} > \mathcal{M}_A^{ha}$ (Sec. 3.4). And the

remaining content of person A is directly propagated by multiplying \mathcal{M}_{SAB}^{hr} with \mathcal{I}_A . In the end, we concatenate $\tilde{\mathcal{I}}_{SAB}^{ha}$, $\tilde{\mathcal{I}}_{SAB}^{hr}$, and $\tilde{\mathcal{I}}_{SAB}^{hc}$ to obtain $\tilde{\mathcal{I}}_{SAB}$.

To facilitate readability, we present our symbol naming conventions in the following enumeration:

- Sign. \mathcal{T} and \mathcal{S} are the teacher and student models; \mathcal{I} , \mathcal{M} , and \mathcal{P} are the image, mask (parsing), and pose.
- Subscript. A and B represent the attribution to person A and B ; AB represents the attribution to a new person A who wears a garment identical to person B ; S and T represent the result predicted by the student model and teacher model; p and w are the parsing reasoning model and flow warping model.
- Superscript. c is the garment-in-shop; hc , ha , and hr are the garment, upper body skin, and remaining category for a person; \sim represents a predicted result whose ground truth is the symbol without \sim .

3.2. The Transfer Parsing Reasoning Teaching

3.2.1. Parsing Reasoning Insight

Garment transfer is a complex computer vision task that attempts to transfer garments from person B to another person A , involving various shape-level and content-level tasks. To alleviate the computational burden of a single model in performing these multi-level tasks, we prioritize the transfer parsing reasoning at the shape level, as it offers the critical shape guidance required for downstream tasks. This transfer parsing has the garment-agnostic features of person A and the transferred garment features of person B .

The fundamental challenge of transfer parsing reasoning lies in how to effectively entangle the garment feature of person B with the pose feature of person A , such that the garment conforms to the global pose feature of person A while preserving its original style and category. This presents a significant challenge for both traditional fully supervised learning and self-supervised learning approaches. In the case of fully supervised learning, acquiring ground truth data where person A wears the garment of person B is essential, but such data is rarely available in practice. Alternatively, in the case of self-supervised learning, the garment features undergo pose augmentation and the model is trained to entangle this augmented garment feature with its original pose feature. However, as data augmentation alone is insufficient to disentangle the original pose feature from the garment, the entanglement learning is prone to degenerate the plain mapping, leading to unreliable reasoning during the testing phase.

In a similar vein, albeit with greater accessibility, virtual try-on wears the garment-in-shop on a person, and we introduce a corresponding try-on parsing reasoning task. As garment-in-shop does not have any inherent pose features, through the exploitation of paired person parsing and garment-in-shop mask data, the entanglement of garment features and pose features can be effectively learned via self-supervised learning.

Assuming the parsing of person A and B are denoted as \mathcal{M}_A , \mathcal{M}_B , and their corresponding garment-in-shop masks are represented as \mathcal{M}_A^c , \mathcal{M}_B^c , we employ the try-on parsing reasoning model \mathcal{T}_p and the transfer parsing reasoning model \mathcal{S}_p as the teacher and student models, respectively. Specifically, we train the teacher model in a self-supervised manner to reason the try-on parsing \mathcal{M}_{TAB} . Thereafter, we employ knowledge distillation to train the student model to perform transfer parsing \mathcal{M}_{SAB} .

3.2.2. Teacher Try-on Parsing Reasoning Model

We exploit the pre-trained Grapy-ML [22] to extract person parsing \mathcal{M}_A , \mathcal{M}_B from images \mathcal{I}_A , \mathcal{I}_B . To facilitate subsequent processing, the person parsing categories are grouped into background, hair, face, upper body skin, upper garment, lower garment, and thigh. Additionally, the pre-trained Densepose model [23] is utilized to extract the dense pose features \mathcal{P}_A , \mathcal{P}_B from images \mathcal{I}_A , \mathcal{I}_B . We adopt U2-Net as the backbone of \mathcal{T}_p , which is proficient in capturing multiscale contextual information and is well-suited for the given reasoning task.

As described in Sec. 3.2.1, the objective of \mathcal{T}_p is to entangle shape features of a new garment-in-shop with pose features of the person while also propagating garment-agnostic features of the person. Achieving this necessitates providing independent priors for each feature. Accordingly, we leverage \mathcal{M}_A^c and \mathcal{P}_A to represent the garment shape and person pose, respectively. Since the upper body skin and background categories entangle with the garment category, including them in garment-agnostic features can hinder entanglement learning. Therefore, we exclude these categories from the parsing \mathcal{M}_A and merge the remaining ones into \mathcal{M}_A^{hr} , which depicts the garment-agnostic shape in person parsing. During the self-supervised training, we concatenate $\mathcal{M}_A^c, \mathcal{P}_A, \mathcal{M}_A^{hr}$ and feed them into the model \mathcal{T}_p to predict $\tilde{\mathcal{M}}_A$, which is supervised with the ground truth \mathcal{M}_A . During testing, we substitute \mathcal{M}_A^c with \mathcal{M}_B^c to predict \mathcal{M}_{TAB} , where person A wears the garment-in-shop B . We denote this process as $\mathcal{M}_{TAB} = \mathcal{T}_p(\mathcal{M}_B^c, \mathcal{P}_A, \mathcal{M}_A^{hr})$ in the formula.

3.2.3. Student Transfer Parsing Reasoning Model

Once the teacher model has been trained, the teacher model \mathcal{T}_p can impart knowledge for supervising the training of the student model \mathcal{S}_p . In this section, we will describe how to implement this teacher-teaches-student process.

Typically, when a teacher teaches a student how to solve a problem, they first introduce the basic knowledge and mechanism, followed by a solution procedure from implicit to explicit, and provide feedback to supervise the student’s learning. If the student aims to become proficient at solving this type of problem, they must practice more through self-study. Drawing inspiration from this, we delicately design the knowledge distillation between parsing reasoning models as three phases: feature knowledge teaching, response knowledge teaching, and self-study phase.

We adopt the same backbone in \mathcal{S}_p as in \mathcal{T}_p . During the feature and response knowledge teaching phase, \mathcal{S}_p is conditioned on \mathcal{M}_B^{hc} , \mathcal{P}_A , and \mathcal{M}_A^{hr} . Due to the unaligned pose of person B in \mathcal{M}_B^{hc} compared to \mathcal{M}_B^c , transfer parsing reasoning poses a greater challenge compared to try-on parsing reasoning. As Fig. 3 shows, the encoder in the backbone is responsible for feature extraction and position awareness. However, since the input between the teacher and student models differs, their learned knowledge in the encoder may not be identical. On the other hand, the decoder in the backbone is responsible for entangling semantic features and reconstructing the parsing structure, and the teacher and student models share the same objective for it. Therefore, we propose to distill the decoder’s knowledge from \mathcal{T}_p to supervise the training of \mathcal{S}_p .

Specifically, we focus on the layers ‘hx6’, ‘hx5d’, ‘hx4d’, ‘hx3d’, ‘hx2d’, and ‘hx1d’¹ in the decoder, which represent a sequence of outputs ranging from coarse to fine. As Fig. 4 shows, it indicates that the global pose and overall shape are learned at the early layers, ‘hx6’ and ‘hx5d’, which are considered basic knowledge for reasoning. Subsequently, the model starts to re-establish human structure and distinguish categories at the intermediate layers, ‘hx4d’, ‘hx3d’, and ‘hx2d’, with particular attention to the boundary and overall shape of the garment and upper body skin, which represent the entanglement of the garment and pose features. Finally, at layer ‘hx1d’, our

¹These signs are derived from the official U2-Net code (<https://github.com/NathanUA/U-2-Net>).

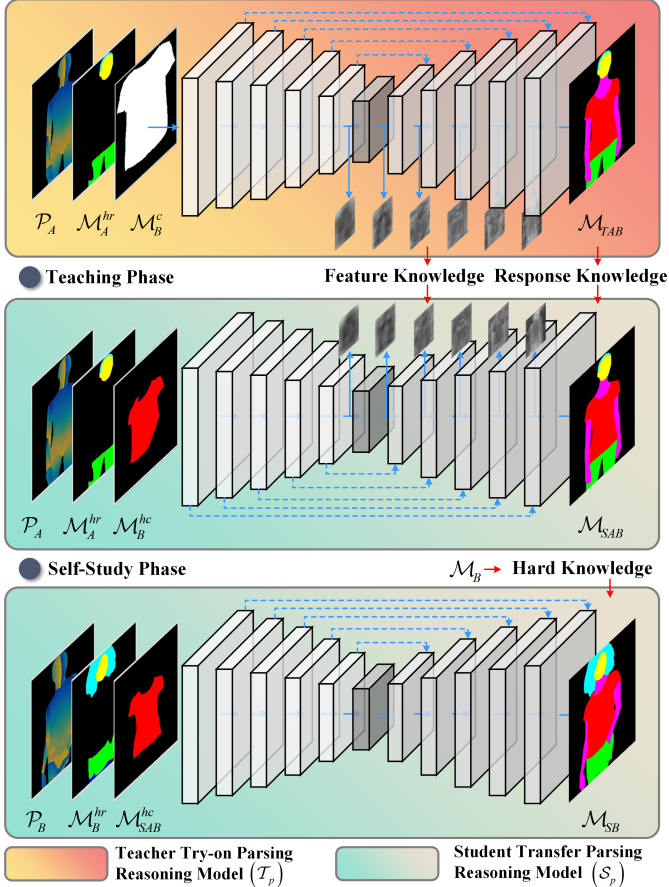


Figure 3: Transfer parsing reasoning teaching. The pre-trained teacher model provides the feature and response knowledge to supervise the training of student model. The student model then advances its reasoning capability by learns the hard knowledge in the self-study phase.

models refine the shape of garment-agnostic categories by fusing low-level shape information from skip connections. During the first stage, we only distilled knowledge from layers 'hx6', 'hx5d', which indirectly supervises S_p at the extraction of hidden knowledge of garment style and target pose. During the second stage, we distilled knowledge from all layers, which supervises S_p at the entanglement of semantic features and reconstruction of parsing spatial relationships.

During the response knowledge teaching phase, we distill soft knowledge in the form of a heat map instead of using one-hot coding. Since the soft tar-

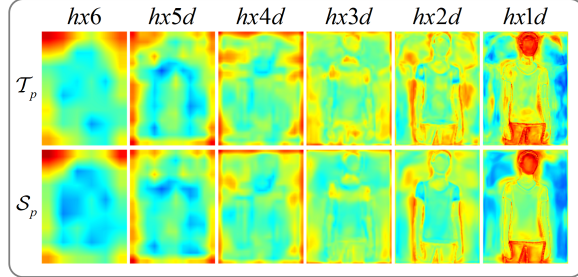


Figure 4: The heat maps of feature knowledge.

get represented by \mathcal{M}_{TAB} is not equivalent to the ground truth, \mathcal{S}_p is able to acquire hard knowledge through self-study after the teaching phase, thereby improving its overall reasoning capacity and facilitating the correction of teaching errors. Specifically, we split the garment category mask \mathcal{M}_{SAB}^{hc} from \mathcal{M}_{SAB} , re-transfer it onto person B , and supervise the reasoning result by the ground truth \mathcal{M}_B . It is described as $\mathcal{M}_{SB} = \mathcal{S}_p(\mathcal{P}_B, \mathcal{M}_B^{hr}, \mathcal{M}_{SAB}^{hc})$ in the formula.

3.2.4. Teaching Procedure

[Algorithm 1](#) summarizes the teaching procedure of reasoning transfer parsing. To distinguish the teaching phase, we employ epoch intervals and utilize distinct combinations of objective functions ℓ_p across the various phases. Specifically, ℓ_{pf} represents the feature loss, defined as [\(1\)](#), where α_T^i and α_S^i correspond to the feature maps at the i -th layer of 'hx6', 'hx5d', 'hx4d', 'hx3d', 'hx2d', 'hx1d', with N denoting the layer quantity. Additionally, we define ℓ_{pd} and ℓ_{ps} as the distillation loss and self-study loss as outlined in [\(2\)](#) and [\(3\)](#).

$$\ell_{pf} = \sum_i^N \|\alpha_T^i - \alpha_S^i\|_1 \quad (1)$$

$$\ell_{pd} = \|\mathcal{M}_{TAB} - \mathcal{M}_{SAB}\|_1 \quad (2)$$

$$\ell_{ps} = \|\mathcal{M}_{SB} - \mathcal{M}_B\|_1 \quad (3)$$

Algorithm 1 The teaching procedure of reasoning transfer parsing.

Input: pre-trained $\mathcal{T}_p; \mathcal{P}_A; \mathcal{P}_B; \mathcal{M}_A; \mathcal{M}_B; \mathcal{M}_B^c$; epoch intervals e_0, e_1, e_2, e_3 ;
hyper parameters $\lambda_1, \lambda_2, \lambda_3$;

- 1: \mathcal{T}_p reasons $\mathcal{M}_{TAB}, \{\alpha_T^i\}_{i=1}^{i=6} = \mathcal{T}_p(\mathcal{M}_B^c, \mathcal{P}_A, \mathcal{M}_A^{hr})$;
- 2: \mathcal{S}_p reasons $\mathcal{M}_{SAB}, \{\alpha_S^i\}_{i=1}^{i=6} = \mathcal{S}_p(\mathcal{M}_B^{hc}, \mathcal{P}_A, \mathcal{M}_A^{hr})$;
- 3: **for** $e = 1 \cdots e_3$ **do**
- 4: **if** $e < e_1$ **then**
- 5: calculate $\ell_{pf}(N = 2)$ and $\ell_p = \lambda_1 \ell_{pf}$;
- 6: **else if** $e_1 < e < e_2$ **then**
- 7: calculate $\ell_{pf}(N = 6)$ and $\ell_p = \lambda_1 \ell_{pf}$;
- 8: **else if** $e_2 < e < e_3$ **then**
- 9: calculate $\ell_{pf}(N = 6), \ell_{pd}$ and $\ell_p = \lambda_1 \ell_{pf} + \lambda_2 \ell_{pd}$;
- 10: **else**
- 11: calculate $\ell_{pf}(N = 6), \ell_{pd}, \ell_{ps}$ and $\ell_p = \lambda_1 \ell_{pf} + \lambda_2 \ell_{pd} + \lambda_3 \ell_{ps}$;
- 12: **end if**
- 13: **end for**
- 14: backward ℓ_p and optimize \mathcal{S}_p ;

3.3. Garment Warping Teaching

3.3.1. Garment Warping Insight

After reasoning the transfer parsing \mathcal{M}_{SAB} , we exploit it as a shape prior and guide the garment warping, which enables the garment \mathcal{I}_B^{hc} of person B to conform to the target shape \mathcal{M}_{SAB}^{hc} . To achieve this, there are differentiable warping tools available such as STN [24], TPS [25], and optical flow [26], which learn affine transformation, coarse-grained grid movement, and pixel displacement, respectively, with varying degrees of freedom. However, for garment transfer, the warping needs to match the garment shape with the target shape in another pose while preserving the garment’s style and texture. Thus, the fine-grained optical flow is the most suitable tool for this task.

Although we derive the target shape for garment warping, the ground truth of garment warping \mathcal{I}_{AB}^{hc} remains unavailable. Supervising the training of the flow warping model for garment transfer with only shape information may lead to distortion and loss of garment semantic information. Therefore, adequate supervision with content information is crucial for estimating high-DOF optical flow. As paired data $(\mathcal{I}_A^c, \mathcal{I}_A^{hc})$ is available, we can train the flow warping model for virtual try-on in a self-supervised manner, and we supervise the flow warping model for garment transfer with both shape and

content information by distilling knowledge from the flow warping model for virtual try-on.

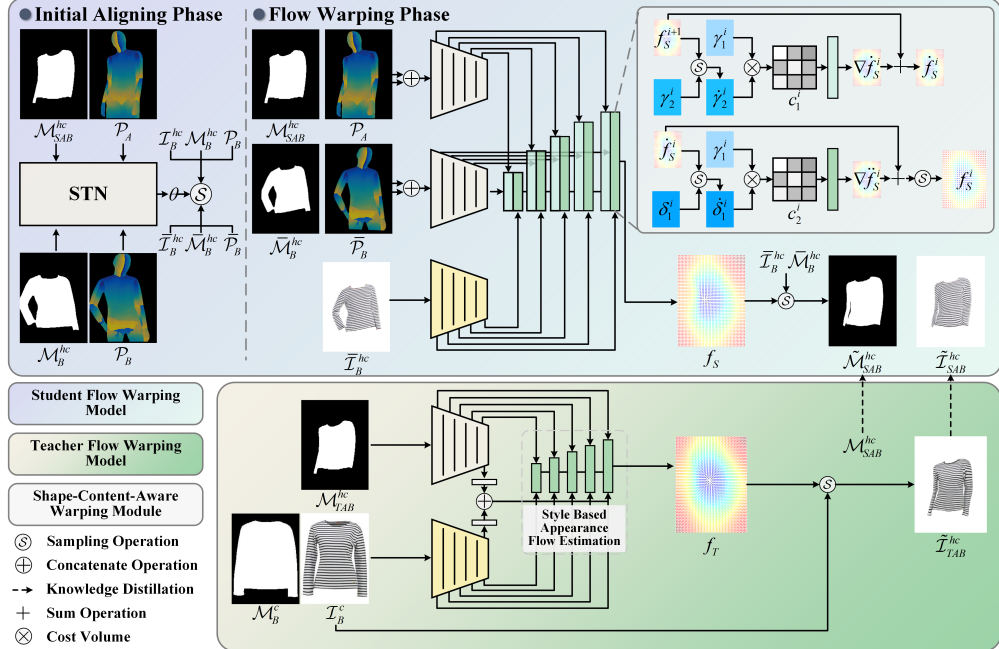


Figure 5: Flow warping teaching. The student flow warping model comprises an initial aligning phase and a flow warping phase. The initial aligning phase learns an affine transformation to facilitate the position mapping, while the flow warping phase focuses on estimating a fine-grained flow to enable precise matching of the transferred garment with the target shape. The training of the student flow warping model is supervised by the shape information \mathcal{M}_{SAB}^{hc} and the distilled content information $\tilde{\mathcal{I}}_{TAB}^{hc}$.

Specifically, as Fig. 5 shows, we leverage the parser-based version of FSV [12] as the teacher flow warping model \mathcal{T}_w , which is capable of estimating global style-based flow and refining flow locally. During its training phase, we represent the human and garment utilizing \mathcal{M}_A^{hc} and $(\mathcal{M}_A^c, \mathcal{I}_A^c)$, and exploit the ground truth \mathcal{I}_A^{hc} to supervise the warping result $\tilde{\mathcal{I}}_A^{hc}$. Once \mathcal{T}_w is trained, we exploit it to warp garment-in-shop B onto person A . i.e. $\tilde{\mathcal{I}}_{TAB}^{hc} = \mathcal{T}_w(\mathcal{M}_{TAB}^{hc}, \mathcal{M}_B^c, \mathcal{I}_B^c)$. With the aid of the supervision information $\mathcal{M}_{SAB}^{hc}, \tilde{\mathcal{I}}_{TAB}^{hc}$ at the shape and content levels, we delicately devise a student flow warping model for garment transfer, inspired by the progressive flow estimation technique in [11], which has the initial aligning phase and the flow warping phase.

3.3.2. Initial Aligning Phase

To address the garment warping problem effectively, we divide it into two subtasks, namely position mapping and shape adjustment. The former task modifies the global position of the garment by scaling, translation, and rotation, while the latter adjusts the local shape to match the target shape precisely using non-rigid warping. For virtual try-on applications, the garment-in-shop usually has a standard pose and a high pixel ratio, as shown in Fig. 6(a), which enables the flow warping model to perform both position mapping and shape adjustment tasks. However, for garment transfer, as shown in Fig. 6(b), the diversity of cropping and pose in the person image may cause the transferred garment to deviate significantly from the target shape in terms of both position and shape. To address this issue, we propose to utilize STN to perform position mapping independently, as shown in Fig. 6(c), which reduces the learning burden of the subsequent flow warping task. Furthermore, due to the locality of CNN, the flow warping model is not able to capture the long-range shape dependence, which may lead to distortion during precise shape matching, as shown in Fig. 6(d). However, the initial aligning phase can mitigate this issue by applying the global affine transformation.

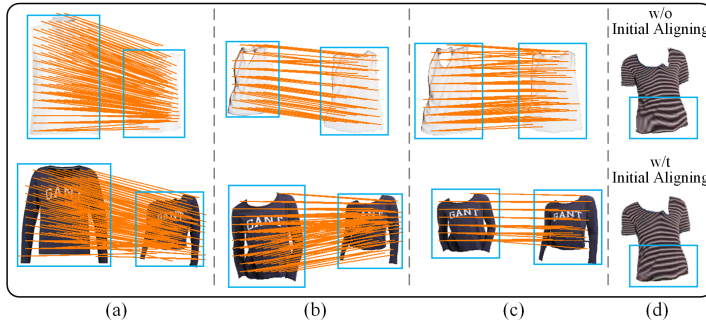


Figure 6: The position mapping and shape adjustment tasks. (a) virtual try-on; (b) garment transfer without initial aligning; (c) garment transfer after initial aligning; (d) shape adjustment comparison.

Though the paired shape representation $(\mathcal{M}_{SAB}^{hc}, \mathcal{M}_B^{hc})$ is available for the initial aligning, the binary shape representation lacks semantic information, we rely on the dense poses to provide the weak semantic information. Specifically, we feed $\mathcal{M}_{SAB}^{hc}, \mathcal{P}_A, \mathcal{M}_B^{hc}, \mathcal{P}_B$ into STN to obtain an affine transformation matrix $\theta \in \mathbb{R}^{3 \times 3}$, which is then applied to the transferred garment

representation $\mathcal{I}_B^{hc}, \mathcal{M}_B^{hc}, \mathcal{P}_B$ to obtain the aligned transferred garment representation $\bar{\mathcal{I}}_B^{hc}, \bar{\mathcal{M}}_B^{hc}, \bar{\mathcal{P}}_B$.

3.3.3. Flow Warping Phase

After the initial aligning, the flow warping phase learns correspondence from coarse to fine levels and estimates a refined flow to accurately warp garment $\bar{\mathcal{I}}_B^{hc}$ to target shape \mathcal{M}_{SAB}^{hc} precisely. To achieve this, the shared encoder E_γ extracts the pyramid feature maps $\{\gamma_1^i\}_{i=1}^{i=5}$ and $\{\gamma_2^i\}_{i=1}^{i=5}$ from weak-semantic shape representation $\{\mathcal{M}_{SAB}^{hc}, \mathcal{P}_A\}$ and $\{\bar{\mathcal{M}}_B^{hc}, \bar{\mathcal{P}}_B\}$ at five downsampling layers. The encoder E_δ has the same structure as E_γ but does not share weights, which extracts the pyramid feature maps $\{\delta_1^i\}_{i=1}^{i=5}$ from $\bar{\mathcal{I}}_B^{hc}$. Consequently, we obtain the paired shape feature maps $\{\gamma_1^i, \gamma_2^i\}$ and the paired content-shape feature maps $\{\gamma_1^i, \delta_1^i\}$, which serve as the condition of the subsequent shape-content-aware warping module (SCAW).

Five SCAWs learn the correspondence between feature maps at the shape level and content level. Each SCAW consists of a shape-aware stage and a content-aware stage. For convenience, we index the downsampling layers of encoders from $i = 1$ to $i = 5$ and index SCAW from $i = 5$ to $i = 1$. Consequently, the i -th SCAW has the same scale as the i -th downsampling layer of encoders and is conditioned on the last flow f_S^{i+1} , γ_1^i , γ_2^i , and δ_1^i . At the shape-aware stage, we first warp γ_2^i to $\dot{\gamma}_2^i$ via f_S^{i+1} and calculate the shape cost volume c_1^i using $\dot{\gamma}_2^i$ and γ_1^i as described in [27]. We then estimate the shape flow residual ∇f_S^i using four Conv2d+LeakyRelu combinations and add it to f_S^i to obtain the shape-aware flow \dot{f}_S^i . At the content-aware stage, we similarly warp δ_1^i to $\dot{\delta}_1^i$ via \dot{f}_S^i and calculate the content cost volume c_2^i using $\dot{\delta}_1^i$ and γ_1^i . The content flow residual $\nabla \ddot{f}_S^i$ is estimated using another four Conv2d+LeakyRelu combinations and added to \dot{f}_S^i to obtain the upsampled output f_S^i . Moreover, the first SCAW module initializes the flow by calculating c_1^i and c_2^i from $\{\gamma_1^i, \gamma_2^i\}$ and $\{\gamma_1^i, \delta_1^i\}$.

By this means, the flow is revised from coarse to fine progressively, and the pixel-level f_S is estimated at the last SCAW. Finally, f_S warps $\bar{\mathcal{I}}_B^{hc}, \bar{\mathcal{M}}_B^{hc}$ to $\tilde{\mathcal{I}}_{SAB}^{hc}, \tilde{\mathcal{M}}_{SAB}^{hc}$.

3.3.4. Objective Function

During training the student flow warping model, we formulate its objective function as (4), where ℓ_w consists of the initial aligning loss ℓ_{wi} , shape content loss ℓ_{ws} , and regularization loss ℓ_{wr} .

$$\ell_w = \ell_{wi} + \ell_{ws} + \ell_{wr} \quad (4)$$

ℓ_{wi} punishes the global shape matching in the initial aligning phase, which consists of two items as (5). The former item punishes the shape error between $\bar{\mathcal{M}}_B^{hc}$ and \mathcal{M}_{SAB}^{hc} , whereas the latter encourages the garment pixel ratio of $\bar{\mathcal{M}}_B^{hc}$ to be similar to \mathcal{M}_{SAB}^{hc} , where H and W represent the height and width of masks; λ_4 and λ_5 are weights.

$$\ell_{wi} = \lambda_4 \left\| \bar{\mathcal{M}}_B^{hc} - \mathcal{M}_{SAB}^{hc} \right\|_1 + \lambda_5 \left\| \sum_{x,y}^{H,W} \bar{\mathcal{M}}_B^{hc} - \sum_{x,y}^{H,W} \mathcal{M}_{SAB}^{hc} \right\|_1 \quad (5)$$

ℓ_{ws} supervises the knowledge distillation from \mathcal{T}_w to \mathcal{S}_w , which consists of two items as (6). The first item punishes the shape error between $\tilde{\mathcal{M}}_{SAB}^{hc}$ and \mathcal{M}_{SAB}^{hc} , while the second and third items punish the image difference between $\tilde{\mathcal{I}}_{TAB}^{hc}$ and $\tilde{\mathcal{I}}_{SAB}^{hc}$ at both the pixel and perceptual levels, where $\phi(\cdot)$ is the VGG loss function. We adopt the pre-trained VGG-19 model [28] to calculate $\phi(\cdot)$ at the 'relu1_1', 'relu2_1', 'relu3_1', and 'relu4_1' layers. $\lambda_6, \lambda_7, \lambda_8$ are weights.

$$\ell_{ws} = \lambda_6 \left\| \tilde{\mathcal{M}}_{SAB}^{hc} - \mathcal{M}_{SAB}^{hc} \right\|_1 + \lambda_7 \left\| \tilde{\mathcal{I}}_{SAB}^{hc} - \tilde{\mathcal{I}}_{TAB}^{hc} \right\|_1 + \lambda_8 \left\| \sum_{i=0}^4 \phi(\tilde{\mathcal{I}}_{SAB}^{hc}) - \phi(\tilde{\mathcal{I}}_{TAB}^{hc}) \right\|_1 \quad (6)$$

ℓ_{wr} regularizes the flow displacement and encourages flow coordination, which consists of two items as (7). We exploit both the one-order constraint in [12] and the second-order constraint in [11] to be ℓ_{wr1} and ℓ_{wr2} . λ_9 and λ_{10} are weights.

$$\ell_{wr} = \lambda_9 \ell_{wr1} + \lambda_{10} \ell_{wr2} \quad (7)$$

3.4. Arm Regrowth

During garment transfer, the shape of the upper body skin may also undergo changes. Therefore, it is crucial to determine an appropriate upper body skin to achieve transfer realism after garment warping. Based on a comparison of the upper body skin mask \mathcal{M}_A^{ha} of person A with the target upper body skin mask \mathcal{M}_{SAB}^{ha} , this task is divided into two cases: covering existing skin or exposing new skin. As shown in Fig. 7, the former scenario

involves simply multiplying \mathcal{M}_{SAB}^{ha} with \mathcal{I}_A . However, the latter scenario presents a difficult task that cannot be resolved through pixel-level operations. Consequently, it is imperative to design a model capable of reasoning about new upper body skin, which has been designated as 'arm regrowth'.

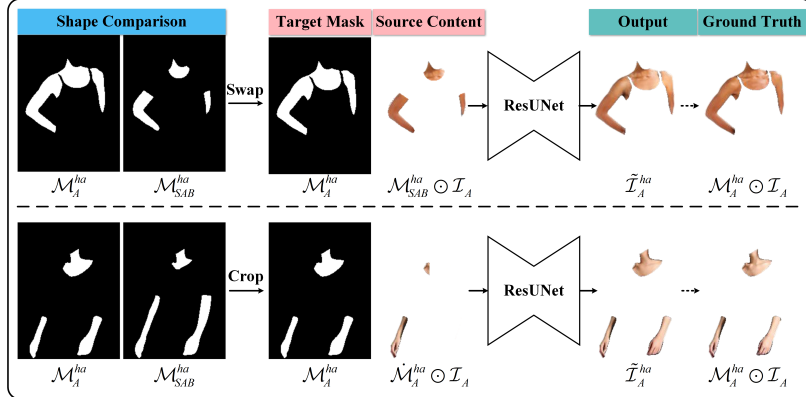


Figure 7: Two cases in training G_r .

The arm regrowth model G_r is trained using an innovative training approach. In the training phase, both scenarios involving exposing new skin are achieved by adjusting the input. For the former scenario, the source and target masks are swapped, where \mathcal{M}_A^{ha} and $\mathcal{M}_{SAB}^{ha} \odot \mathcal{I}_A^{ha}$ are taken as the target mask and source content. They are then fed into ResUnet [29] to predict $\tilde{\mathcal{I}}_A^{ha}$, guided by the ground truth $\mathcal{M}_A^{ha} \odot \mathcal{I}_A$. For the latter scenario, \mathcal{M}_A^{ha} is randomly cropped to $\dot{\mathcal{M}}_A^{ha}$, with the half-plane shape removed on the horizontal or vertical axis. Using \mathcal{M}_A^{ha} and $\dot{\mathcal{M}}_A^{ha} \odot \mathcal{I}_A$ as the target mask and source content, they are fed into the same ResUnet to predict $\tilde{\mathcal{I}}_A^{ha}$. In the testing phase, \mathcal{I}_A^{ha} , \mathcal{M}_{SAB}^{ha} are inputted into the pre-trained ResUnet to yield $\tilde{\mathcal{I}}_{SAB}^{ha}$, which is denoted as $\tilde{\mathcal{I}}_{SAB}^{ha} = G_r(\mathcal{I}_A^{ha}, \mathcal{M}_{SAB}^{ha})$ in the formula.

We design its objective function ℓ_r as (8) where ℓ_{r1}, ℓ_{rc} are the L1 and content losses; $\lambda_{11}, \lambda_{12}$ are weights. ℓ_{r1} and ℓ_{rc} are defined as (9) and (10) where $\phi(\cdot)$ is the same as (6).

$$\ell_r = \lambda_{11}\ell_{r1} + \lambda_{12}\ell_{rc} \quad (8)$$

$$\ell_{r1} = \left\| \tilde{\mathcal{I}}_A^{ha} - \mathcal{M}_A^{ha} \odot \mathcal{I}_A \right\|_1 \quad (9)$$

$$\ell_{rc} = \left\| \sum_{i=1}^4 \phi \left(\tilde{\mathcal{I}}_A^{ha} \right) - \sum_{i=1}^4 \phi \left(\mathcal{M}_A^{ha} \odot \mathcal{I}_A \right) \right\|_1 \quad (10)$$

4. Experiment

4.1. Implementation Details

We exploit the Zalando dataset [1] to train and evaluate our proposed method². This dataset is further cleaned so that the training set and test set consist of 11565 and 1698 paired data with a resolution of 256×192 . We randomly match person A and B to form the garment transfer pair. All experiments were conducted on a single 3090 NVIDIA GPU by Adam optimizer. We present the hyperparameters of garment transfer models in the training phase in Table 1 and provide the model complexity in Table 2.

Table 1: The hyperparameters in training garment transfer models.

Network	LR	Iterations	Batch	Weights
\mathcal{S}_p	$2 \times e^{-4}$	18.1 K	16	$\lambda_1 = 0.1, \lambda_2 = 60.0, \lambda_3 = 60.0$
\mathcal{S}_w	$1 \times e^{-4}$	72.2 K	8	$\lambda_4 = 0.6, \lambda_5 = 6 \times e^{-3}, \lambda_6 = 2.0, \lambda_7 = 1.0, \lambda_8 = 0.2, \lambda_9 = 6.0, \lambda_{10} = 1 \times e^{-2}$
G_r	$1 \times e^{-4}$	18.1 K	16	$\lambda_{11} = 10.0, \lambda_{12} = 0.2$

Table 2: The model complexity.

Model	\mathcal{S}_p	\mathcal{S}_w	G_r	All
Params/M	44.10	26.66	43.90	114.66
FLOPs/G	28.62	55.05	21.86	105.53

4.2. Ablation Study

4.2.1. Transfer Parsing Reasoning

Metrics In this section, we conduct the ablation study of transfer parsing reasoning to verify the necessity of knowledge distillation in training

²We have gotten the using permission for the research purpose from its author Xintong Han.

\mathcal{S}_p , the rationality of the phase setting in the teaching procedure, and the appropriateness of the backbone and pose form for this task. We exploit the intersection over union (IoU) and class pixel accuracy (CPA) as metrics, both of which range from 0 to 1. Since the entanglement between the garment and pose is crucial in transfer parsing reasoning, we focus on the metrics values of the garment and upper body skin categories. Thus, we compare \mathcal{M}_{SAB} with \mathcal{M}_{TAB} to verify the knowledge distillation effect, denoted as $\text{IoU}(\mathcal{M}_{TAB}^{ha}, \mathcal{M}_{SAB}^{ha})$, $\text{IoU}(\mathcal{M}_{TAB}^{hc}, \mathcal{M}_{SAB}^{hc})$, $\text{CPA}(\mathcal{M}_{TAB}^{ha}, \mathcal{M}_{SAB}^{ha})$, and $\text{CPA}(\mathcal{M}_{TAB}^{hc}, \mathcal{M}_{SAB}^{hc})$. And we compare \mathcal{M}_{SB} with \mathcal{M}_B to verify the reasoning rationality with ground truth, denoted as $\text{IoU}(\mathcal{M}_{SB}^{ha}, \mathcal{M}_B^{ha})$, $\text{IoU}(\mathcal{M}_{SB}^{hc}, \mathcal{M}_B^{hc})$, $\text{CPA}(\mathcal{M}_{SB}^{ha}, \mathcal{M}_B^{ha})$, and $\text{CPA}(\mathcal{M}_{SB}^{hc}, \mathcal{M}_B^{hc})$.

The Necessity of Knowledge Distillation As described in Sec. 3.2.1, without knowledge distillation, we train \mathcal{S}_p in a self-supervised manner as comparisons. Specifically, during the training phase, \mathcal{S}_p is conditioned on augmented \mathcal{M}_A^{hc} , \mathcal{M}_A^{hr} , and \mathcal{P}_A , while the ground truth \mathcal{M}_A is leveraged to supervise the output of \mathcal{S}_p . The traditional data augmentation operations, including affine transformation, cropping, and flipping, are used in three different combinations: affine transformation; affine transformation and cropping; and affine transformation, cropping, and flipping. To further improve the performance, we adopted the cycle consistency strategy from [10], which involves dressing \mathcal{M}_B^{hc} onto person A to generate $\tilde{\mathcal{M}}_{AB}$ and then dressing $\tilde{\mathcal{M}}_{AB}^{hc}$ onto person B again, supervised by the ground truth \mathcal{M}_B . The quantitative and qualitative results are shown in Fig. 8 and Fig. 9, respectively.

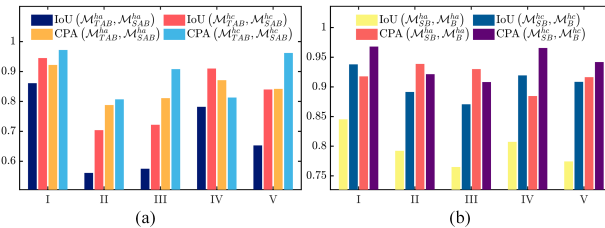


Figure 8: Quantitative results in verifying the necessity of knowledge distillation. Cases I-V are the baseline; affine transformation, affine transformation and cropping; affine transformation, cropping, and flipping; and cycle consistency.

For cases II and III, the translation invariance of CNN allows \mathcal{S}_p to learn the pose feature from \mathcal{M}_A^{hc} even after affine transformation and cropping. This enables the transfer parsing reasoning to degenerate into rigid trans-

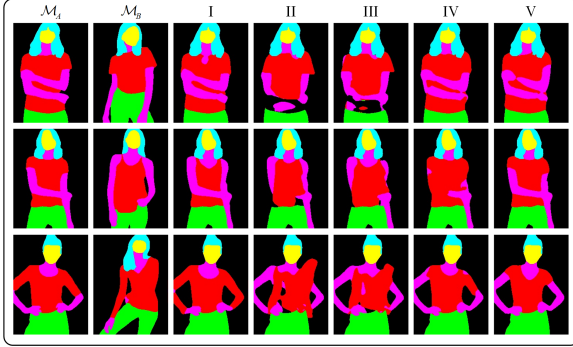


Figure 9: Qualitative results in verifying the necessity of knowledge distillation. Cases I-V are the same as Fig. 8.

formation learning, resulting in \mathcal{M}_B^{hc} being simply pasted onto \mathcal{M}_A^{hr} to form \mathcal{M}_{SAB} , leading to a reduction of 34.03% and 24.55% in IoU ($\mathcal{M}_{TAB}^{ha}, \mathcal{M}_{SAB}^{ha}$) and IoU ($\mathcal{M}_{TAB}^{hc}, \mathcal{M}_{SAB}^{hc}$). For case IV, the flipping operation goes against the CNN translation invariance, but the style and shape of the garment are completely changed. In consequence, \mathcal{S}_p has a poor performance in capturing these features, leading to \mathcal{M}_{SAB} having the shape and style deviation, especially when \mathcal{M}_B^{hc} is in a complex pose. And IoU ($\mathcal{M}_{TAB}^{ha}, \mathcal{M}_{SAB}^{ha}$), IoU ($\mathcal{M}_{TAB}^{hc}, \mathcal{M}_{SAB}^{hc}$) reduce by 9.17% and 3.49%, respectively. For case V, the CNN model tends to take a shortcut, but cycle consistency fails to supervise the intermediate result $\tilde{\mathcal{M}}_{AB}$. Therefore, cycle consistency prefers less variation, which results in the garment style in \mathcal{M}_{SAB} being improperly changed to a T-shirt, irrespective of the style of the transferred garment. This leads to a reduction of CPA ($\mathcal{M}_{TAB}^{ha}, \mathcal{M}_{SAB}^{ha}$) and CPA ($\mathcal{M}_{TAB}^{hc}, \mathcal{M}_{SAB}^{hc}$) by 9.17% and 3.49%, respectively.

The Rationality of Phase Setting As described in Sec. 3.2.4, we design four cases to verify the rationality of phase setting. The former two cases are designated to verify the effectiveness of the feature knowledge teaching phase, while the latter two cases are intended to verify the self-study phase. As Fig. 10(a) shows, in case I, we follow Algorithm. 1 until epoch e_3 , while in case II, we only distill response knowledge within the epoch range of $[0, e_3]$. Case III is designed to follow Algorithm. 1 until epoch e_4 , and case IV follows Algorithm. 1 within the epoch range of $[0, e_3]$, but only distills the feature and response knowledge during $[e_3, e_4]$. The quantitative and qualitative results are shown in Fig. 10 and Fig. 11, respectively.

Compared with case I, case II does not include the reasoning process

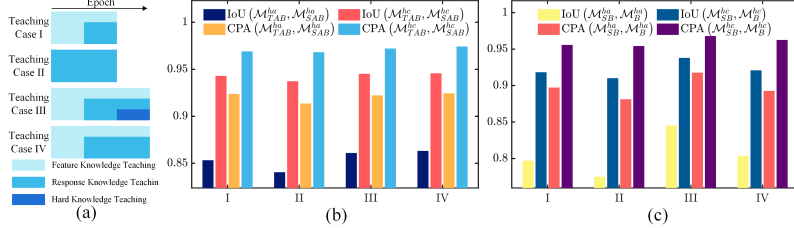


Figure 10: Quantitative results in verifying the phase setting rationality. (a) four cases; (b) the teacher similarity; (c) the ground truth similarity.

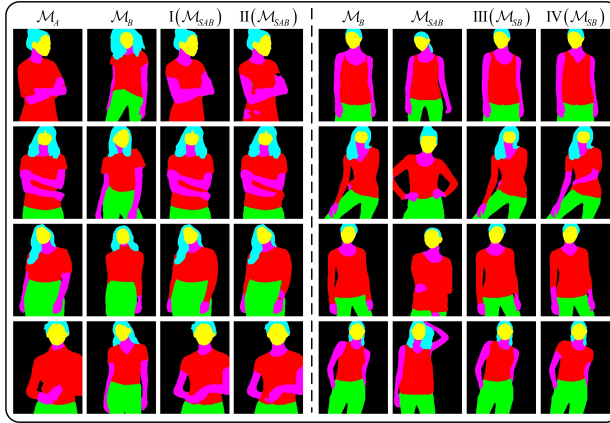


Figure 11: Qualitative comparisons in verifying the phase setting rationality.

teaching, it only simulates \mathcal{T}_p at the response level but neglects to learn the semantic feature entanglement and human structure reconstruction from \mathcal{T}_p . Consequently, case II fails to comprehend the semantic features of garment style and global human pose, leading to fragmentary arm and sleeve variations, and a 1.49% and 1.10% decrease in $\text{IoU}(\mathcal{M}_{TAB}^{ha}, \mathcal{M}_{SAB}^{ha})$ and $\text{CPA}(\mathcal{M}_{TAB}^{ha}, \mathcal{M}_{SAB}^{ha})$, respectively. To compare case III and case IV, we adopt the more challenging reasoning $\mathcal{M}_{SB} = \mathcal{S}_p(\mathcal{P}_B, \mathcal{M}_B^{hr}, \mathcal{M}_{SAB}^{hc})$. Case IV simulates \mathcal{T}_p so excessively that it is misled by wrong reasoning instances, such as comprehending a long-sleeve garment as a short-sleeve one. As a result, case IV has poor performance in reasoning \mathcal{M}_{SB} compared to reasoning \mathcal{M}_{SAB} . In contrast, case III can revise the wrong teaching in the self-study phase and has a similar performance in reasoning \mathcal{M}_{SB} and \mathcal{M}_{SAB} . It indicates that the reasoning of case III is closer to the ground truth rather than just following \mathcal{T}_p . Additionally, the quantitative results of case III in rea-

soning \mathcal{M}_{SB} show a significant increase, indicating that the self-study phase allows \mathcal{S}_p to be more stable by feeding more transfer instances.

The Appropriateness of Backbone and Pose Form We compare the appropriateness of different backbones for the parsing reasoning task, including U2-Net [30], U-Net [31], ResUnet [29], and UNet++ [32]. We compare the function of DensePose and OpenPose in reasoning. The quantitative and qualitative results are shown in Fig. 12 and Fig. 13, respectively.

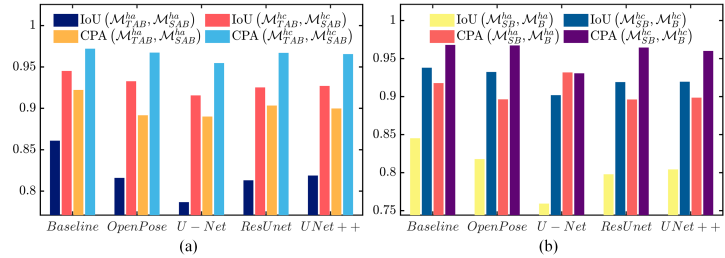


Figure 12: Quantitative results in verifying the appropriateness of backbone and pose form. (a) the teacher similarity; (b) the ground truth similarity.

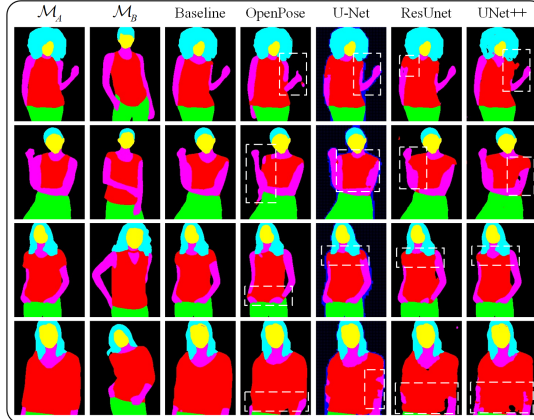


Figure 13: Qualitative comparisons in verifying the appropriateness of backbone and pose form.

The U2-Net backbone, which utilizes a deep architecture by nesting U-Net, is adept at capturing semantic features of garments and poses. It excels in reconstructing and propagating local details by fusing multiscale features, resulting in better preservation of arm shape and garment details compared

to other backbones, as indicated by a reduction of IoU ($\mathcal{M}_{SB}^{hc}, \mathcal{M}_B^{hc}$) and IoU ($\mathcal{M}_{SB}^{hc}, \mathcal{M}_B^{hc}$) by 6.87% and 2.60%, respectively. Thus, U2-Net is deemed more suitable for the parsing reasoning task among the considered backbones. On the other hand, OpenPose only provides information on joint positions, and thus, fails to reconstruct fine arm shapes due to the lack of arm shape prior. In contrast, DensePose, which provides human structure and shape prior, results in an increase of IoU ($\mathcal{M}_{SAB}^{ha}, \mathcal{M}_{TAB}^{ha}$) and IoU ($\mathcal{M}_B^{ha}, \mathcal{M}_{SB}^{ha}$) by 5.51% and 3.34%, respectively.

4.2.2. Garment Warping

Metrics In this section, we verify the necessity of knowledge distillation in training, the appropriateness of warping method, and the rationality of phase setting. Similar to Sec. 4.2.1, we compare $\tilde{\mathcal{I}}_{SAB}^{hc}$ with $\tilde{\mathcal{I}}_{TAB}^{hc}$ to verify the knowledge distillation and compare $\tilde{\mathcal{I}}_{SB}^{hc}$ with \mathcal{I}_B^{hc} to verify the garment warping authenticity to the ground truth. We exploit the low-level full-reference metrics, high-level full-reference metrics, and no-reference subjective metric. The low-level full-reference metrics consist of MSE, SSIM, and PSNR; the high-level full-reference metrics consist of FID [33] and LPIPS [34]; the no-reference subjective metric is IS [35].

The Necessity of Knowledge Distillation As outlined in Sec. 3.3.1, we investigate the necessity of knowledge distillation in training \mathcal{S}_w by comparing three cases. The first case is our baseline. The second case involves training \mathcal{S}_w solely using shape information \mathcal{M}_{SAB}^{hc} , without knowledge distillation from \mathcal{T}_w . The third case involves training \mathcal{S}_w by enforcing cycle consistency, as described in Sec. 4.2.1. The comparison results are presented in Fig. 14 and 15.

Case II only warps the boundary of \mathcal{I}_B^{hc} towards \mathcal{M}_{SAB}^{hc} , while the internal structure of the garment remains unchanged because the shape information does not guide warping inside the garment. In contrast, in case I, the distilled content information $\tilde{\mathcal{I}}_{TAB}^{hc}$ supervises the warp of the internal content of the garment to reflect pose changes. This results in a more realistic warp that conforms to the global semantics of garment transfer. As a result, MSE ($\tilde{\mathcal{I}}_{TAB}^{hc}, \tilde{\mathcal{I}}_{SAB}^{hc}$) and LPIPS ($\tilde{\mathcal{I}}_{TAB}^{hc}, \tilde{\mathcal{I}}_{SAB}^{hc}$) increase by 30.96% and 36.56% in case II. It is worth noting that case II performs well when warping $\tilde{\mathcal{I}}_{SAB}^{hc}$ to $\tilde{\mathcal{I}}_{SB}^{hc}$ because warping from $\tilde{\mathcal{I}}_B^{hc}$ to $\tilde{\mathcal{I}}_{SAB}^{hc}$ involves less change. This further indicates that case II almost does not change the internal content of the garment. Case III faces an intermediate result supervision problem and

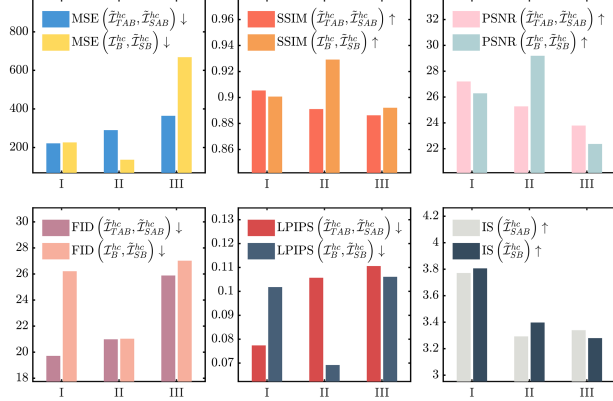


Figure 14: Quantitative results in verifying the necessity of knowledge distillation. Cases I-III are baseline, supervision only with shape information, and training in cycle consistency.

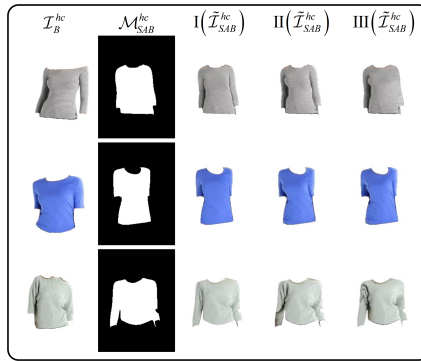


Figure 15: Qualitative results in verifying the necessity of knowledge distillation.

cannot prevent the model from shortcutting. Consequently, during training, case III is likely to collapse, resulting in reductions of 14.91% and 13.84% in $\text{PSNR}(\tilde{\mathcal{I}}_{SB}^{hc}, \mathcal{I}_B^{hc})$ and $\text{IS}(\tilde{\mathcal{I}}_{SB}^{hc}, \mathcal{I}_B^{hc})$, respectively.

The Appropriateness of Warping Method As described in Sec. 3.3.1, we evaluate the appropriateness of mapping, TPS deformation, and TPS deformation+render for garment transfer. To ensure a fair comparison, we employ the same knowledge distillation pipeline when training these methods. Specifically, for the mapping method, we leverage \mathcal{T}_w as the teacher model and the texture module of SwapNet [3] as the student model. The student model is conditioned on \mathcal{M}_{SAB}^{hc} and the garment embedding, which is obtained by ROI pooling of \mathcal{I}_B^{hc} ; In the case of TPS deformation, we exploit

the clothes warping module of ACGPN [7] as the teacher and student models. The student model is conditioned on \mathcal{M}_B^{hc} and \mathcal{M}_{SAB}^{hc} . In the case of TPS deformation + render, we further input the warped result of case III into a refinement network, which is the same as ACGPN. The quantitative and qualitative results are shown in Fig. 16 and 17.

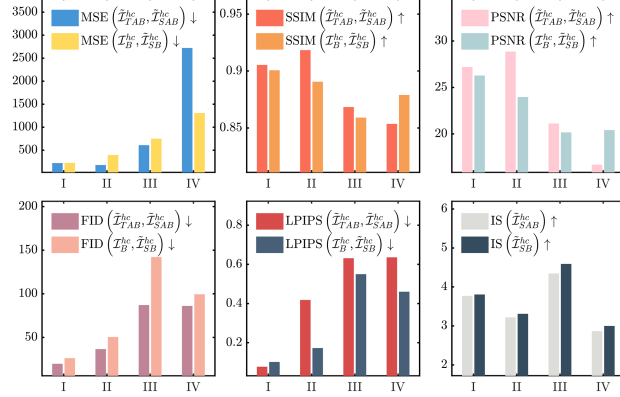


Figure 16: Quantitative results in verifying the appropriateness of warping method. Cases I-IV are baseline, mapping, TPS deformation, and TPS deformation + render.

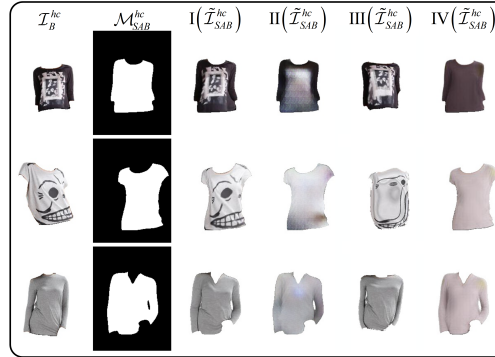


Figure 17: Qualitative results in verifying the appropriateness of warping method.

Case II is burdened with complex texture mapping due to variations in the texture and decoration of the garment. Consequently, an average color is padded into the target shape, resulting in blurred texture and discarded decoration. This causes an increase of 85.54% and 92.51% in $\text{FID}(\tilde{\mathcal{I}}_{TAB}^{hc}, \tilde{\mathcal{I}}_{SAB}^{hc})$ and $\text{FID}(\tilde{\mathcal{I}}_{SB}^{hc}, \mathcal{I}_B^{hc})$, respectively. As TPS deformation has a low DOF, while

TPS deformation works well in obtaining a coarse warped result for garments with standard poses and large scales in virtual try-on, fine warping from pose to pose is necessary for garment transfer. Therefore, case III cannot accurately warp the garment to match the target shape and tends to produce distortion, leading to an increase of 175.44% and 341.51% in $\text{MSE}(\tilde{\mathcal{I}}_{TAB}^{hc}, \tilde{\mathcal{I}}_{SAB}^{hc})$ and $\text{FID}(\tilde{\mathcal{I}}_{TAB}^{hc}, \tilde{\mathcal{I}}_{SAB}^{hc})$, respectively. In case IV, rendering texture is also a challenge, and the poor warped result and unaligned \mathcal{I}_B^{hc} cause training instability and collapse, resulting in a reduction of $\text{IS}(\tilde{\mathcal{I}}_{SAB}^{hc})$ by 24.01%.

The Rationality of Phase Setting To confirm the effectiveness of the initial aligning phase, we input the unaligned shape pair directly into the flow warping phase. Similarly, to evaluate the architecture of the flow warping phase, we replace it with the same architecture as \mathcal{T}_w . Quantitative and qualitative results are shown in Fig. 18 and 19.

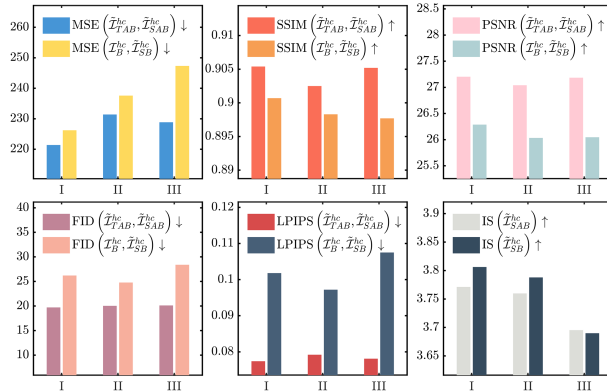


Figure 18: Quantitative results in verifying the rationality of phase setting. Cases I-III are baseline, without the initial aligning phase, and with the same architecture as \mathcal{T}_w

In case II, position mapping and shape adjustment are accomplished through high-DOF flow warping. However, when \mathcal{M}_B^{hc} is significantly smaller than \mathcal{M}_{SAB}^{hc} , it tends to excessively stretch the local region to match the target shape precisely. In contrast, case I aligns \mathcal{I}_B^{hc} globally with \mathcal{M}_{SAB}^{hc} to achieve a similar scale and position. Subsequently, flow warping is leveraged to adjust the shape accurately. As a result, the texture blur and garment style variation are reduced, and $\text{MSE}(\tilde{\mathcal{I}}_{TAB}^{hc}, \tilde{\mathcal{I}}_{SAB}^{hc})$ and $\text{LPIPS}(\tilde{\mathcal{I}}_{TAB}^{hc}, \tilde{\mathcal{I}}_{SAB}^{hc})$ decrease by 4.32% and 2.27%. In case III, the FSV modulates the pose and

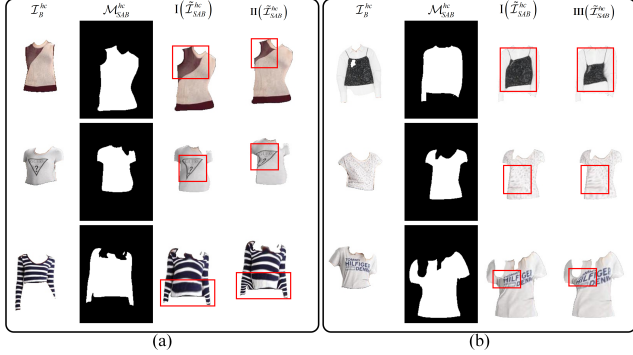


Figure 19: Qualitative results in verifying the rationality of phase setting.

garment features to estimate a coarse try-on result, which performs well in virtual try-on without parsing reasoning. However, our garment transfer pipeline provides the fined target shape, rendering the mechanism of FSV unnecessary. Conversely, the innovation of case I learns correspondence at the shape and content level, emphasizing semantic alignment and consistency in garment warping. As a result, $\tilde{\mathcal{I}}_{SAB}^{hc}$ is more realistic, and $IS(\tilde{\mathcal{I}}_{SAB}^{hc})$ and $IS(\tilde{\mathcal{I}}_{SB}^{hc})$ increase by 2.05% and 3.15%.

4.2.3. Arm Regrowth

In this section, we aim to demonstrate the effectiveness of our training strategy for arm regrowth. As described in Sec. 3.4, due to the unavailability of ground truth data for arm regrowth, we can only train G_r in a self-supervised manner when ablating our training strategy. Specifically, similar to Sec. 4.2.1, we employ three operation combinations to augment \mathcal{I}_A^{ha} during the training phase, and G_r is conditioned on the augmented \mathcal{I}_A^{ha} and \mathcal{M}_A^{ha} to predict $\tilde{\mathcal{I}}_A^{ha}$. During the testing phase, all models are conditioned on \mathcal{I}_A^{ha} , \mathcal{M}_{SAB}^{ha} , and \mathcal{M}_A^{ha} and follow the data processing method in Sec. 3.4 for the quantitative comparison. The qualitative and quantitative comparisons are shown in Fig. 20 and Table 3.

The task of arm regrowth can be divided into two sub-tasks: propagating the original arm part and reasoning the new arm part. In case II, the augmented \mathcal{I}_A^{ha} is misaligned with \mathcal{M}_A^{ha} through an affine transformation, resulting in G_r padding the overall target shape with the semantic features of \mathcal{I}_A^{ha} . Consequently, the results of case II discard high-frequency details such as the hand and neck by inferring rather than propagating the content at the

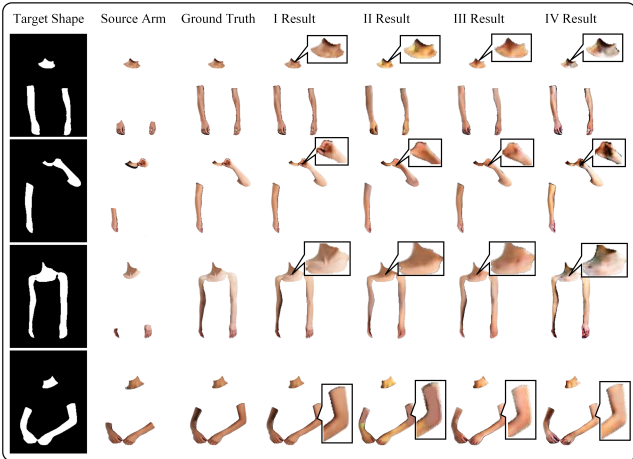


Figure 20: Qualitative results in arm regrowth. Cases I-IV are baseline; affine transformation; affine transformation and cropping, affine transformation, cropping and flipping.

Table 3: Quantitative results in arm regrowth.

	MSE	PSNR	SSIM	FID	LPIPS	IS
Case I	19.63	36.65	0.980	5.96	0.017	2.47
Case II	91.55	29.28	0.942	22.72	0.055	2.62
Case III	74.29	30.11	0.949	16.50	0.047	2.55
Case IV	88.84	29.53	0.949	20.82	0.051	2.62

overlapped region between \mathcal{M}_{SAB}^{ha} and \mathcal{M}_A^{ha} . In case III, new arm exposure is more realistically simulated in the training phase by using random cropping, resulting in a relative reduction of 18.85% and 14.54% in MSE and LPIPS respectively when compared to case II. Nevertheless, the results of case III still exhibit artifacts and blurring. Case IV further impedes the propagation of the original arm part by using random flipping, resulting in worse results compared to case III. Unlike these data augmentation techniques, case I aims to enable the input conditions of the training and testing phases as similar as possible to perform well in both sub-tasks, leading to significant quantitative results.

4.3. Comparison

4.3.1. Virtual Try-on Method

Baseline We compare our method with virtual try-on methods in garment transfer. Virtual try-on methods consist of VITON [1], CP-VTON [2], ACGPN [7], DCTON [10], PF-AFN [11], and FSV [12]. We adopt their official implementations and checkpoint pre-trained on the Zalando dataset³.

Metrics We compare the performance of different methods for transferring the garment from \mathcal{I}_B to \mathcal{I}_A to obtain $\tilde{\mathcal{I}}_{AB}$. In order to perform this transfer, virtual try-on methods are conditioned on both \mathcal{I}_A and \mathcal{I}_B^{hc} . As the ground truth for $\tilde{\mathcal{I}}_{AB}$ is unavailable, we present several examples in Fig. 21 and evaluate their subjective image quality using IS [35] and hyperIQA [36] in Table 4. To conduct a more detailed quantitative comparison, we re-transfer the garment from $\tilde{\mathcal{I}}_{AB}$ to \mathcal{I}_B and utilize \mathcal{I}_B as the ground truth. We also adopt the same metrics as in Sec. 4.2.2. Specifically, we utilize the pre-trained Grapy-ML to extract $\tilde{\mathcal{M}}_{AB}$ from $\tilde{\mathcal{I}}_{AB}$ and yield the transferred garment $\tilde{\mathcal{I}}_{AB}^{hc}$. Subsequently, virtual try-on methods are conditioned on both $\tilde{\mathcal{I}}_{AB}^{hc}$ and \mathcal{I}_B to predict $\tilde{\mathcal{I}}_B$, and the quantitative results are presented in Table 5.

Table 4: Quantitative comparison with virtual try-on methods in garment transfer from \mathcal{I}_B to \mathcal{I}_A .

	Ours	VITON	CP-VTON	ACGPN	DCTON	PF-AFN	FSV
IS↑	2.75	2.39	2.42	2.50	2.42	2.31	2.38
hyperIQA↑	35.94	31.81	28.20	27.11	29.49	28.80	27.92

Virtual try-on methods are limited in their ability to capture position and style features of transferred garments, resulting in warped garments that do not align with the transfer parsing and yielding artifacts in the unaligned region. In contrast, our method precisely warps \mathcal{I}_B^{hc} towards \mathcal{M}_{SAB}^{hc} through initial aligning and flow warping. Additionally, these virtual try-on methods cannot avoid being affected by the garment shape features of \mathcal{I}_A when reasoning a proper transfer parsing, leading to \mathcal{I}_B^{hc} warping toward \mathcal{I}_A^{hc} . In contrast, our method infers a parsing that entangles the shape feature of the transfer garment with the pose feature of another person, while maintaining

³Since CP-VTON does not release its official code, we adopt the most starred unofficial code on Github (<https://github.com/sergeywong/cp-vton>)

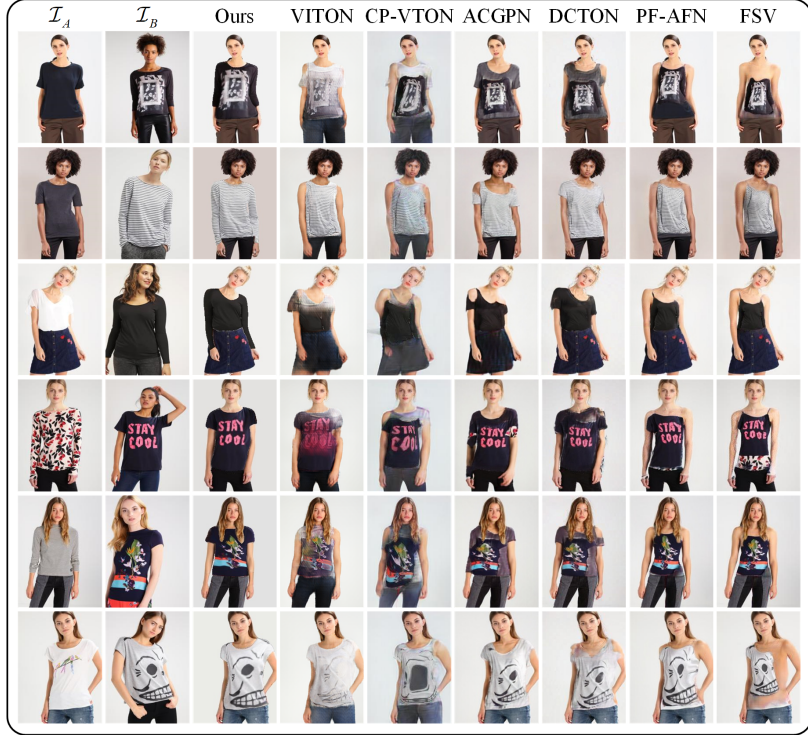


Figure 21: Qualitative comparison with virtual try-on methods.

Table 5: Quantitative comparison with virtual try-on methods in garment transfer from $\tilde{\mathcal{I}}_{AB}$ to \mathcal{I}_B .

	MSE \downarrow	PSNR \uparrow	SSIM \uparrow	FID \downarrow	LPIPS \downarrow	IS \uparrow
Ours	389.029	23.57	0.863	19.14	0.108	2.734
VITON	3867.18	16.15	0.700	75.91	0.258	2.374
CP-VTON	1853.72	16.27	0.712	53.10	0.244	2.266
ACGPN	647.72	21.31	0.825	27.64	0.147	2.496
DCTON	770.71	20.27	0.814	32.18	0.159	2.455
PF-AFN	1359.94	18.15	0.823	46.15	0.176	2.280
FSV	1711.46	17.12	0.820	56.50	0.191	2.317

their inherent features. This allows our results to be more aligned with the intended garment transfer. In quantitative comparisons, our method achieves the highest scores of IS and hyperIQA in garment transfer from \mathcal{I}_B to \mathcal{I}_A .

Moreover, our MSE and FID are approximately 20.89% and 34.37% lower than those of other virtual try-on methods in garment transfer from $\tilde{\mathcal{I}}_{AB}$ to \mathcal{I}_B .

4.3.2. Garment Transfer Method

Baseline We compare our method with other state-of-the-art garment transfer methods, which consist of SwapNet [3], CT-Net [4], and PASTA-GAN [14]. We trained SwapNet on the Zalando dataset with an unofficial implementation⁴. CT-Net requires paired images of the same person wearing the same garment in different poses for training. Therefore, we utilized its official implementation and pre-trained checkpoint on Deepfashion2 [6] and test it on the Zalando dataset. In addition, PASTA-GAN adopts its official implementation and pre-trained checkpoint.

Metrics Similar to Sec. 4.3.1, in the garment transfer from \mathcal{I}_B to \mathcal{I}_A , we enumerate some examples and their subjective image quality assessments in Fig. 22 and Table 6, respectively. In the garment transfer from $\tilde{\mathcal{I}}_{AB}$ to \mathcal{I}_B , we provide quantitative results in Table 7.

Table 6: Quantitative comparison with garment transfer methods in garment transfer from \mathcal{I}_B to \mathcal{I}_A .

	Ours	SwapNet	CT-Net	PASTA-GAN
IS \uparrow	2.75	2.73	2.48	2.71
hyperIQA \uparrow	35.94	27.20	33.24	32.93

Table 7: Quantitative comparison with garment transfer methods in garment transfer from $\tilde{\mathcal{I}}_{AB}$ to \mathcal{I}_B .

	MSE \downarrow	PSNR \uparrow	SSIM \uparrow	FID \downarrow	LPIPS \downarrow	IS \uparrow
Ours	389.029	23.57	0.863	19.14	0.108	2.734
SwapNet	1705.66	16.31	0.677	67.45	0.269	2.557
CT-Net	2980.83	13.86	0.626	86.69	0.352	2.266
PASTA-GAN	621.76	21.07	0.845	15.03	0.105	2.725

⁴<https://github.com/andrewjong/SwapNet>

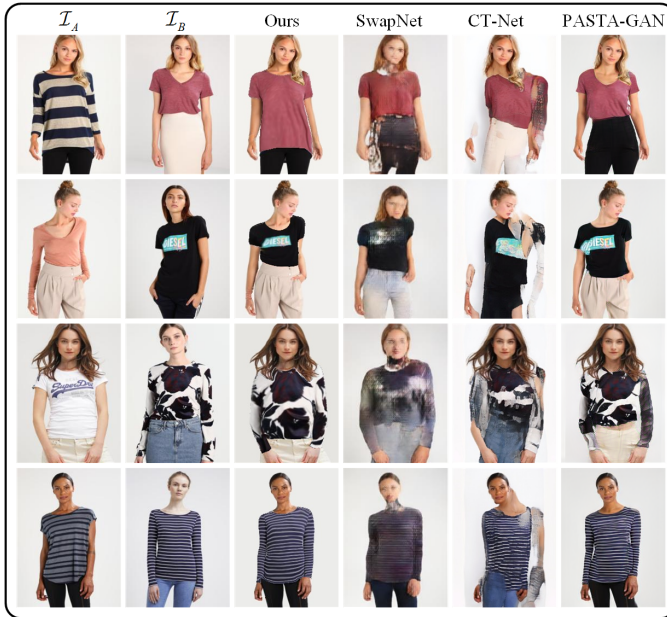


Figure 22: Qualitative comparison with garment transfer methods.

SwapNet learns category embedding to infer pixel content, which places a significant learning burden on the CNN model. When the garment being transferred has intricate texture and local details, SwapNet tends to blur textures and discard high-frequency details, resulting in unrealistic outcomes, particularly in face and garment regions. This leads to a decrease in hyper-IQA by 24.31%. CT-Net’s robustness on the Zalando dataset is low without re-training it, and its training strategy falls under self-supervision learning, which causes differences in input between the training and testing phases. Moreover, the arm inferring mechanism of CT-Net is implicit, making it challenging to handle the cases of exposing new skin as the first and second rows in [Fig. 22](#). PASTA-GAN disentangles the garment with the pose by dividing the garment image into several patches, but the semantics between patches are discontinuous when reconstructing the garment structure as the target pose. This creates an apparent boundary between patches, leading to unrealistic transfer results, with SSIM decreasing by 10.61%. In contrast, our method warps the garment instead of mapping it, has an explicit arm re-growth mechanism, and attains the highest scores of IS and hyperIQA among the garment transfer methods discussed.

As Fig. 23 shows, when the transferred garment is in an extreme pose, the garment warping continuity makes it challenging to tear down the cover region and leave a blank, and the sleeve of the transferred garment is put in an incorrect position. To avoid transfer failure, the user should not leverage such a person image as garment condition. As unobserved content inference is still a challenging topic in the community, our future work will involve combining warping with rendering to handle the transferred garment occlusion.



Figure 23: Failure cases.

5. Conclusion

This paper proposes a novel garment transfer method supervised with knowledge distillation from virtual try-on. Our method first reasons the transfer parsing to provide shape prior for downstream tasks. We employ a multi-phase teaching strategy to supervise the transfer parsing reasoning model during training. When transferring a garment to another person, it learns the response and feature knowledge from the try-on parsing reasoning model. When transferring the garment back to its owner, it absorbs the hard knowledge from the ground truth. Guided by the transfer parsing, we map the position of the transferred garment mask toward the target shape to prevent distortion. Afterward, we estimate a progressive flow for precise warping of the garment by learning shape and content correspondence. To ensure that the boundary and internal structure of the garment are changed reasonably, we supervise the training of the flow warping model using target shape and warping knowledge from virtual try-on. To better preserve body features in the transfer result, we propose a well-designed training strategy for the arm regrowth task, which propagates the source arm part and reasons

the new arm part. Experiments demonstrate that our method has state-of-the-art performance compared with other virtual try-on and garment transfer methods in garment transfer, especially for preserving garment texture and body features.

6. Declaration of competing interest

The authors declare that they have no known competing financial interests or personal relationships that could have appeared to influence the work reported in this paper.

7. Acknowledgements

This research was supported by the National Key R&D Program of China (No. 2018YFB1700700).

References

- [1] X. Han, Z. Wu, Z. Wu, R. Yu, L. S. Davis, Viton: An image-based virtual try-on network, in: Proceedings of the IEEE/CVF Conference on Computer Vision and Pattern Recognition (CVPR), 2018, pp. 7543–7552.
- [2] B. Wang, H. Zheng, X. Liang, Y. Chen, L. Lin, M. Yang, Toward characteristic-preserving image-based virtual try-on network, in: Proceedings of the European Conference on Computer Vision (ECCV), 2018, pp. 589–604.
- [3] A. Raj, P. Sangkloy, H. Chang, J. Lu, D. Ceylan, J. Hays, Swapnet: Garment transfer in single view images, in: Proceedings of the European Conference on Computer Vision (ECCV), 2018, pp. 666–682.
- [4] F. Yang, G. Lin, Ct-net: Complementary transferring network for garment transfer with arbitrary geometric changes, in: Proceedings of the IEEE/CVF Conference on Computer Vision and Pattern Recognition (CVPR), 2021, pp. 9899–9908.
- [5] S. Choi, S. Park, M. Lee, J. Choo, Viton-hd: High-resolution virtual try-on via misalignment-aware normalization, in: Proceedings of the IEEE/CVF Conference on Computer Vision and Pattern Recognition (CVPR), 2021, pp. 14131–14140.

- [6] Y. Ge, R. Zhang, X. Wang, X. Tang, P. Luo, Deepfashion2: A versatile benchmark for detection, pose estimation, segmentation and re-identification of clothing images, in: Proceedings of the IEEE/CVF Conference on Computer Vision and Pattern Recognition (CVPR), 2019, pp. 5337–5345.
- [7] H. Yang, R. Zhang, X. Guo, W. Liu, W. Zuo, P. Luo, Towards photo-realistic virtual try-on by adaptively generating-preserving image content, in: Proceedings of the IEEE/CVF Conference on Computer Vision and Pattern Recognition (CVPR), 2020, pp. 7850–7859.
- [8] M. R. Minar, T. T. Tuan, H. Ahn, P. Rosin, Y.-K. Lai, Cp-vton+: Clothing shape and texture preserving image-based virtual try-on, in: CVPR Workshops, 2020.
- [9] A. Neuberger, E. Borenstein, B. Hilleli, E. Oks, S. Alpert, Image based virtual try-on network from unpaired data, in: Proceedings of the IEEE/CVF Conference on Computer Vision and Pattern Recognition (CVPR), 2020, pp. 5184–5193.
- [10] C. Ge, Y. Song, Y. Ge, H. Yang, W. Liu, P. Luo, Disentangled cycle consistency for highly-realistic virtual try-on, in: Proceedings of the IEEE/CVF Conference on Computer Vision and Pattern Recognition (CVPR), 2021, pp. 16928–16937.
- [11] Y. Ge, Y. Song, R. Zhang, C. Ge, W. Liu, P. Luo, Parser-free virtual try-on via distilling appearance flows, in: Proceedings of the IEEE/CVF Conference on Computer Vision and Pattern Recognition (CVPR), 2021, pp. 8485–8493.
- [12] S. He, Y.-Z. Song, T. Xiang, Style-based global appearance flow for virtual try-on, in: Proceedings of the IEEE/CVF Conference on Computer Vision and Pattern Recognition (CVPR), 2022, pp. 3470–3479.
- [13] T. Issenhuth, J. Mary, C. Calauzènes, Do not mask what you do not need to mask: a parser-free virtual try-on, in: Proceedings of the European Conference on Computer Vision (ECCV), Springer, 2020, pp. 619–635.
- [14] Z. Xie, Z. Huang, F. Zhao, H. Dong, M. Kampffmeyer, X. Liang, Towards scalable unpaired virtual try-on via patch-routed spatially-

adaptive gan, *Advances in Neural Information Processing Systems* 34 (2021) 2598–2610.

- [15] T. Liu, J. Zhang, X. Nie, Y. Wei, S. Wei, Y. Zhao, J. Feng, Spatial-aware texture transformer for high-fidelity garment transfer, *IEEE Transactions on Image Processing* 30 (2021) 7499–7510.
- [16] G. Hinton, O. Vinyals, J. Dean, et al., Distilling the knowledge in a neural network, *arXiv preprint arXiv:1503.02531* 2 (2015).
- [17] S. Zagoruyko, N. Komodakis, Paying more attention to attention: Improving the performance of convolutional neural networks via attention transfer, in: *International Conference on Learning Representations*, 2017.
- [18] F. Ding, Y. Yang, H. Hu, V. Krovi, F. Luo, Dual-level knowledge distillation via knowledge alignment and correlation, *IEEE Transactions on Neural Networks and Learning Systems* (2022).
- [19] J. Liu, B. Li, M. Lei, Y. Shi, Self-supervised knowledge distillation for complementary label learning, *Neural Networks* 155 (2022) 318–327.
- [20] Y. Tian, S. Sun, J. Tang, Multi-view teacher–student network, *Neural Networks* 146 (2022) 69–84.
- [21] Y. Huang, Y. Hao, J. Xu, B. Xu, Compressing speaker extraction model with ultra-low precision quantization and knowledge distillation, *Neural Networks* 154 (2022) 13–21.
- [22] H. He, J. Zhang, Q. Zhang, D. Tao, Grapy-ml: Graph pyramid mutual learning for cross-dataset human parsing, in: *Proceedings of the AAAI Conference on Artificial Intelligence*, volume 34, 2020, pp. 10949–10956.
- [23] R. A. Güler, N. Neverova, I. Kokkinos, Densepose: Dense human pose estimation in the wild, in: *Proceedings of the IEEE/CVF Conference on Computer Vision and Pattern Recognition (CVPR)*, 2018, pp. 7297–7306.
- [24] M. Jaderberg, K. Simonyan, A. Zisserman, et al., Spatial transformer networks, *Advances in neural information processing systems* 28 (2015).

- [25] F. L. Bookstein, Principal warps: Thin-plate splines and the decomposition of deformations, *IEEE Transactions on pattern analysis and machine intelligence* 11 (1989) 567–585.
- [26] A. Dosovitskiy, P. Fischer, E. Ilg, P. Hausser, C. Hazirbas, V. Golkov, P. Van Der Smagt, D. Cremers, T. Brox, Flownet: Learning optical flow with convolutional networks, in: *Proceedings of the IEEE/CVF International Conference on Computer Vision (ICCV)*, 2015, pp. 2758–2766.
- [27] E. Ilg, N. Mayer, T. Saikia, M. Keuper, A. Dosovitskiy, T. Brox, Flownet 2.0: Evolution of optical flow estimation with deep networks, in: *Proceedings of the IEEE/CVF Conference on Computer Vision and Pattern Recognition (CVPR)*, 2017, pp. 2462–2470.
- [28] K. Simonyan, A. Zisserman, Very deep convolutional networks for large-scale image recognition, *arXiv preprint arXiv:1409.1556* (2014).
- [29] Z. Zhang, Q. Liu, Y. Wang, Road extraction by deep residual u-net, *IEEE Geoscience and Remote Sensing Letters* 15 (2018) 749–753.
- [30] X. Qin, Z. Zhang, C. Huang, M. Dehghan, O. R. Zaiane, M. Jagersand, U2-net: Going deeper with nested u-structure for salient object detection, *Pattern recognition* 106 (2020) 107404.
- [31] O. Ronneberger, P. Fischer, T. Brox, U-net: Convolutional networks for biomedical image segmentation, in: *International Conference on Medical image computing and computer-assisted intervention*, Springer, 2015, pp. 234–241.
- [32] Z. Zhou, M. M. R. Siddiquee, N. Tajbakhsh, J. Liang, Unet++: Re-designing skip connections to exploit multiscale features in image segmentation, *IEEE transactions on medical imaging* 39 (2019) 1856–1867.
- [33] M. Heusel, H. Ramsauer, T. Unterthiner, B. Nessler, S. Hochreiter, Gans trained by a two time-scale update rule converge to a local nash equilibrium, *Advances in neural information processing systems* 30 (2017).
- [34] R. Zhang, P. Isola, A. A. Efros, E. Shechtman, O. Wang, The unreasonable effectiveness of deep features as a perceptual metric, in: *Proceedings of the IEEE/CVF Conference on Computer Vision and Pattern Recognition (CVPR)*, 2018, pp. 586–595.

- [35] T. Salimans, I. Goodfellow, W. Zaremba, V. Cheung, A. Radford, X. Chen, Improved techniques for training gans, *Advances in neural information processing systems* 29 (2016).
- [36] S. Su, Q. Yan, Y. Zhu, C. Zhang, X. Ge, J. Sun, Y. Zhang, Blindly assess image quality in the wild guided by a self-adaptive hyper network, in: *Proceedings of the IEEE/CVF Conference on Computer Vision and Pattern Recognition (CVPR)*, 2020, pp. 3667–3676.